# Efficient sensitivity analysis of classical Helmholz resonators based on polynomial chaos expansion

Philipp M. Heck[1], Sabine C. Langer[1]

[1] *Institute for Acoustics and Dynamics, 38106 Braunschweig, Germany, Email: philipp.heck@tu-braunschweig.de*

## Introduction

The absorption of airborne sound plays an important role in various applications, e.g. in the targeted influencing of reverberation in room acoustics. Compared to porous absorbers, classic Helmholtz resonators (HR) have the advantage of improved narrow-band absorption behaviour in low frequency ranges. In addition, HRs for low-frequency absorption have comparatively smaller dimensions than porous absorbers, which is also an advantage for lightweight applications, e.g. in aviation. Due to the complex interactions of the parameters in the model, the effects of the individual parameters and their interactions on the acoustic behaviour of HRs can be quantified by a global sensitivity study. The identification of key parameters is crucial for the effective design of absorbers, as the manufacturing and environmental conditions must be linked to them.

This paper is organised as follows: An analytical model based on the transfer matrix method is presented and validated both experimentally and by finite element method. A global sensitivity study using the polynomial chaos expansion is then carried out and the results are summarised with an outlook for future work.

## Classical Helmholtz resonator

### Acoustical model of the Helmholtz resonator

Under the assumption of a plane wave excitation, the transfer matrix method (TMM) is used to describe the 1D acoustical behaviour of a Helmholtz resonator (see Fig. 1). The acoustic system is divided into several layers with different local coordinate systems ($0 < x_i < l_i$). However, different fluid properties are assigned to each layer. The transfer behaviour between the layers is determined using the Helmholtz equations for pressure $p$ and particle velocity $v$ as well as the equilibrium conditions of pressure and volume flow $V = vS$ at the layer boundaries. This results in the following matrix-vector product:

$$\begin{pmatrix} p \\ V \end{pmatrix}_{x=0} = \mathbf{T}_i \begin{pmatrix} p \\ V \end{pmatrix}_{x=l_i} \tag{1}$$

The overall transfer behaviour for a classical HR (see Fig. 1) is then described by a series connection $\prod_{i=1} \mathbf{T}_i$ of the individual layer matrices $\mathbf{T}_i$:

$$\begin{pmatrix} p_1 \\ V_1 \end{pmatrix} = \mathbf{T} \begin{pmatrix} p_3 \\ V_3 \end{pmatrix} \tag{2}$$

with the overall transfer matrix $\mathbf{T}$:

$$\begin{bmatrix} \cos(k_\mathrm{n} l_\mathrm{n}) & j\tilde{Z}_\mathrm{n} \sin(k_\mathrm{n} l_\mathrm{n}) \\ \frac{j}{\tilde{Z}_\mathrm{n}} \cos(k_\mathrm{n} l_\mathrm{n}) & \cos(k_\mathrm{n} l_\mathrm{n}) \end{bmatrix} \begin{bmatrix} \cos(k_\mathrm{c} l_\mathrm{c}) & j\tilde{Z}_\mathrm{c} \sin(k_\mathrm{c} l_\mathrm{c}) \\ \frac{j}{\tilde{Z}_\mathrm{c}} \cos(k_\mathrm{c} l_\mathrm{c}) & \cos(k_\mathrm{c} l_\mathrm{c}) \end{bmatrix}$$

where $k$, $l$, $\tilde{Z}$ denote the wave number, the length of the layer and the characteristic impedance of the neck (index $n$) and the resonator cavity (index $c$). In addition, $j$ describes the imaginary unit. The characteristic impedance $\tilde{Z} = \rho c/S$ describes the ratio of the multiplication of the speed of sound $c$ and density $\rho$ to the cross-sectional area $S$.

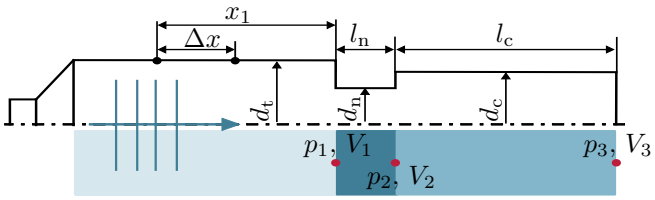


**Figure 1:** Schematic representation of the air volume of a classic Helmholz resonator and the mechanical replacement model, excited by a loudspeaker

As already mentioned, each layer has different material properties. It is assumed that the waveguide and the resonator cavity have the same fluid properties without attenuation effects. Therefore, the temperature-independent ambient density (isochoric condition) is set to $\rho_0 = 1.19 \frac{\mathrm{kg}}{\mathrm{m}^3}$ and the temperature-dependent wave velocity results in [1]:

$$c_0 = \sqrt{\gamma \frac{R_\mathrm{m}}{M} T_0} \tag{3}$$

where $\gamma$ denotes the heat capacity ratio, $R_\mathrm{m}$ the general gas constant, $M$ the molar mass of air and $T_0$ the absolute ambient temperature. The wave number can be calculated by $k = \Omega/c$, where $\Omega$ is the excitation angular frequency. The attenuation effects of the HR are only taken into account in the neck area due to effective material properties. The effective bulk modulus, which describes the effect of thermal exchanges with the frame, is described as follows [2, 8]:

$$K_\mathrm{eff} = \frac{\gamma p_0}{\gamma - (\gamma - 1) F(Pr\Omega)} \tag{4}$$

$$F(Pr\Omega) = \frac{1}{1 + \frac{\phi\sigma}{jPr\Omega\rho_0} G(\sqrt{Pr}s)} \tag{5}$$

$$G(s) = -\frac{s\sqrt{-j}}{4} \frac{J_1(s\sqrt{-j})}{J_0(s\sqrt{-j})} \Big/ \left[1 - \frac{2}{s\sqrt{-j}} \frac{J_1(s\sqrt{-j})}{J_0(s\sqrt{-j})}\right] \tag{6}$$

The quantities $p_0$, $Pr$, $\phi\sigma$ describes the ambient pressure, the Prandtl number and the porosity-weighted flow resistivity, which is defined for a circular hole as $\phi\sigma = 32\eta/d_\mathrm{n}^2$ [2]. The functions $J_0$ and $J_1$ are first kind Bessel functions of the zeroth and first order. For circular holes, the shear wave number $s$ is defined as follows [2, 14]:

$$s = \sqrt{\frac{1}{4} \frac{\rho_0 \Omega}{\eta}} d_\mathrm{n} \tag{7}$$

where $\eta$, $\rho_0$, $d_\mathrm{n}$ denote the air dynamic viscosity, the ambient density and the neck diameter. Since the influence of pressure on dynamic viscosity is negligible, the temperature dependence is described by the Sutherland equation as follows [5]:

$$\eta = \frac{291.15\mathrm{K} + 120\,\mathrm{K}}{T_0 + 120\,\mathrm{K}} \left(\frac{T_0}{293.15\ \mathrm{K}}\right)^{3/2} 18.27\ \mu\mathrm{Pa\,s} \quad (8)$$

Assuming an ideal gas, the Prandtl number is also only a temperature-dependent quantity whose relationship is determined by a polynomial approximation of the material data in [6]:

$$\begin{aligned} Pr =& 2.487 \cdot 10^{-13} t_0^4 - 6.707 \cdot 10^{-10} t_0^3 \\ &+ 6.08 \cdot 10^{-7} t_0^2 - 1.569 \cdot 10^{-4} t_0 + 0.7108 \end{aligned} \quad (9)$$

where $t_0$ describes the ambient temperature.

The viscosity attenuation effect inside holes is taken into account by an effective complex density [2]. Okuzono et al. [12] derive the density - based on models by Guo [14], Maa [11] and Allard [2] - by adapting Crandall's [13] transfer impedance model:

$$Z_t = \frac{\Delta p}{\overline{v}} = j\Omega l_n \rho_0 \left(1 + \frac{\phi\sigma G(s)}{j\Omega\rho_0}\right) + 2\alpha_R R_s + j\Omega\rho_0\delta \quad (10)$$

$$= j\Omega l_n \rho_\mathrm{eff} \quad (11)$$

$$\rho_\mathrm{eff} = \rho_0 (1 + \frac{\phi\sigma}{j\Omega\rho_0} G(s) + \frac{2\alpha_R R_s}{j\Omega l_n \rho_0} + \frac{\delta}{l_n}) \quad (12)$$

where $l_\mathrm{n}$, $R_\mathrm{s}$, $\delta$ describes the length of the neck, the surface resistance and the mass end correction. The surface resistance $R_s = 1/2\sqrt{2\eta\rho_0\Omega}$ describes the frictional losses due to the tangential flow over the plate and $\alpha_R$ is a correction factor for different hole shapes and surface properties (here: $\alpha_R = 4$) [8]. The mass end correction describes the increasing of the kinetic energy due the flow distortion in the vicinity of the opening and is described by [7, 8]:

$$\delta_i = \delta_0 d_\mathrm{n}/2(1 - 1.33\varepsilon_i^{1/2} - 0.07\varepsilon_i + 0.4\varepsilon_i^{3/2}) \quad (13)$$

$$\delta_0 = \frac{\pi/4\ e^{1.2\log(0.13)} + 0.82\ e^{1.2\log(2l_\mathrm{n}/d_\mathrm{n})}}{e^{1.2\log(0.13)} + e^{1.2\log(2l_\mathrm{n}/d_\mathrm{n})}} \quad (14)$$

Since the mass end correction at both ends of the neck are different, the total end correction is the sum of these corrections $\delta = \delta_1 + \delta_2$, but with different perforation ratios $\varepsilon_{1,2}$.

To calculate the frequency-dependent absorption coefficient, the surface impedance of the Helmholtz resonator is first determined, as the reflection depends on an impedance change at the medium boundaries. The surface impedance is defined as the ratio of sound pressure $p_1$ to sound particle velocity $v_1$:

$$\mathrm{Z_{surface}} = \frac{p_1}{v_1} = \frac{\mathbf{T}_{11} p_3 + \mathbf{T}_{12} V_3}{\mathbf{T}_{21} p_3 + \mathbf{T}_{22} V_3} S_\mathrm{t} = \frac{\mathbf{T}_{11}}{\mathbf{T}_{21}} S_\mathrm{t} \quad (15)$$

Since the volume flow $V_3$ must be zero at the end of the HR cavity, the surface impedance is a ratio of the matrix entries of the overall transfer matrix $\mathbf{T}$. The absorption coefficient can then be determined taking into account the mechanical equilibrium and the continuity condition at the boundary between the impedance tube medium and the medium of the HR [1]:

$$\alpha = 1 - \left| \frac{1 - \frac{Z_0}{Z_\mathrm{surface}}}{1 + \frac{Z_0}{Z_\mathrm{surface}}} \right|^2 \quad (16)$$

where $Z_0 = \rho_0 c_0$ describes the characteristic impedance of the ambient air, the waveguide medium.

**Experimental and numerical model validation**

The analytical model is validated to show that the results are very similar to those of an FE model - but with significantly less computational effort - and that both models accurately capture the physical behaviour.

For the experimental validation, the absorption coefficient is measured using the two-microphone method according to ISO 10534-2 and compared with the analytical HR model. The determination of the absorption coefficient [3]:

$$\alpha_\mathrm{meas.} = 1 - \left| \frac{H_{12} - e^{jk_0\Delta x}}{e^{jk_0\Delta x} - H_{12}} e^{2jk_0 x_1} \right|^2 \quad (17)$$

based on the measurement of the amplitude and phase corrected transfer function $H_{12}$ between the two microphone positions (see Fig. 1) and the ambient conditions [3]. Since the standardised estimators for the transfer function $H_{12}$ only suppress the noise on one of both signals, a total-least-squares frequency response estimator $H_\mathrm{v}$ is used [4]:

$$H_\mathrm{v} = \frac{1}{2s_{21}} \left[ (s_{22} - s_{11}) + \sqrt{(s_{11} - s_{22})^2 + 4|s_{12}|^2} \right] \quad (18)$$

with $s_{ii}$, $s_{ij}$ for the auto and cross spectrum of the measured sound pressure level $p_{x_1}$ and $p_{x_1 - \Delta x}$. The validation is based on defined HR nominal values (see Tab. 1); one of the HR samples made of aluminum is shown in Fig. 2. The uncertainties of the manufacturing process and the measuring method are taken into account by measuring 5 manufactured neck samples. The Python-based SciPy library is used to estimate the cross-power spectrum and the power spectral density based on Welch method's. The selected frequency resolution is 1 Hz, the segment length is 22 500 with an overlap of 66.67 %. The specified frequency range is between 100 Hz and 1347 Hz, with a selected sampling rate of 22 500 Hz and a total measurement time of 20 s.

A rotationally symmetric 2D finite element model of the impedance tube air (see Fig. 2) is created in COMSOL Multiphysics 6.3 for the numerical validation. In the frequency domain, the Helmholtz equation is solved under harmonic excitation by an incident pressure field with an amplitude of 1 Pa. Instead of considering viscosity losses and heat conduction effects with linearised Navier-Stokes equations, the previously presented effective material properties (Eq. 4 and Eq. 12) are used in the neck domain. The mass end corrections $\delta$ are neglected as they are implicitly taken into account in the FEM solution by the discretisation of the field problem. Therefore, the selected discretisation in the neck area is finer than in the remaining area (max. element length $d_n/6$). The discretisation of the rest of the structure is based on the resolution of the airborne sound wave at maximum frequency and the requirement of 9 nodes per bending wavelength. The selected ansatz function of the quadratic elements is of the quadratic serendipity type and the considered frequency range and its resolution corresponds to that of the experimental validation. The numerical calculation of the absorption coefficient

$\alpha = 1 - \frac{I_r}{I_i}$ is based on the calculation of the incident sound intensity $I_i$ and the reflected sound intensity $I_r$ at the radiation boundary.

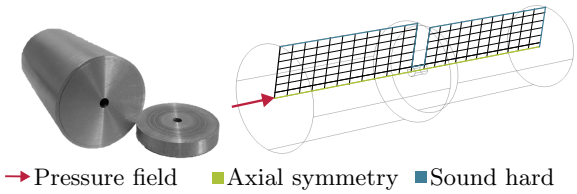


**Figure 2: Left**: Test sample with the nominal values and **right**: Schematic representation of the 2D FE-model

Fig. 3 shows the experimentally determined frequency-dependent absorption behavior, the numerically and the semi-analytically calculated behaviour. The low standard deviation shows the accuracy of the manufacturing process and the measurement method. In addition, the analytical model and the FE-model describe the acoustic behaviour very accurately. The relative deviation of the resonance frequency between experiment and the TMM-model is $\varepsilon_{\mathrm{f_{res}}} = 0.93$ % and the relative deviation of the maximum absorption is $\varepsilon_\alpha = 0.64$ %. The comparison between FEM and measurement shows $\varepsilon_{\mathrm{f_{res}}} = 0.62$ % for the comparison of the resonance frequency and $\varepsilon_\alpha = 0.29$ % for the relative deviation of the maximum absorption.

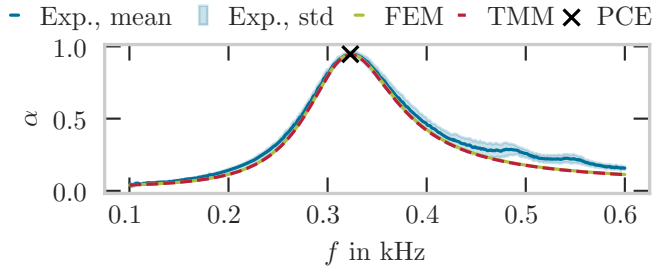


**Figure 3:** Experimental and numerical validation of the TMM; standard deviation based on 5 measurements

## Sensitivity analysis

The term sensitivity analysis refers to a collection of methods for determining the sensitivity of model output variables to their input parameters. This contribution conducts a Sobol analysis, which is a global method to quantify the influence of uncertain input parameters on target model quantity of interest. The Sobol analysis is a varianced based method in which the variance of the model output is decomposed into a sum of parts that relate to individual inputs or groups of inputs [9]. The variance decomposition can be performed because the model output of each square integrable function $Y = M(\mathbf{X})$ can be described with respect to independently distributed input parameters $\mathbf{X} = (X_1, X_2, ..., X_d)$ with a PDF as a sum of elementary functions [9]. The ratio of the partial variances to the total variance $\mathrm{Var}(Y)$ describes the "Sobol indices" [9]:

$$1 = \sum_{i=1}^{d} S_i + \sum_{i<j}^{d} S_{ij} + ... + S_{12...d} \tag{19}$$

$$S_i = \frac{\mathrm{Var}[\mathbb{E}(Y|X_i)]}{\mathrm{Var}(Y)}$$

$$S_{ij} = \frac{\mathrm{Var}[\mathbb{E}(Y|X_i, X_j)]}{\mathrm{Var}(Y)} - S_i - S_j$$

where $S_i$ describes the first-order indices and $S_{ij}$ the second-order indices. A further index is the total Sobol index, which describes the total variance of the model output that can be attributed to the effect of a single input parameter [9]:

$$S_{\mathrm{T_i}} = 1 - \frac{\mathrm{Var}[\mathbb{E}(Y|\mathbf{X}_{-i})]}{\mathrm{Var}(Y)} \tag{20}$$

where $\mathrm{Var}[\mathbb{E}(Y|\mathbf{X}_{-i})]$ denotes the total amount of variance without taking the i-th input parameter into account. If the sum of the first-order Sobol indices is equal to 1, then the input parameters exhibit additive model behaviour and it follows that the total Sobol indices $S_{\mathrm{T}_i}$ are equal to the first-order indices $S_i$. This also means that all parameters show no interaction effects. On contrary, models with interaction effect, directly indicate a non-linear behaviour.

Estimating the Sobol indices via sampling based methods, requires a high number of model calls, an efficient surrogate modelling method, the polynomial chaos expansion (PCE), is used [9]. The truncated PCE surrogate model results in [9]:

$$Y = M(\mathbf{X}) \approx \sum_{\mathbf{a}\in\mathbb{N}^d} c_{\mathbf{a}} \Psi_{\mathbf{a}}(\mathbf{X}),\ \mathbf{a} = (a_1, ..., a_d),\ a_i \in \mathbb{N} \tag{21}$$

where $\mathbf{a}$, $c_{\mathbf{a}}$, $\Psi_{\mathbf{a}}$ describes the multi-indices, the coefficients and multivariate orthonormal polynomials with respect to the distributions $\mathbf{X}$ [9]. Based on a PCE surrogate, the Sobol indices of any order are determined by a combination of the squared coefficients of the surrogate [9].

In this paper, the sensitivities of the resonance frequency and the maximum absorption coefficient are determined. For this purpose, two PCE surrogate models are designed for a defined parameter range using the python library UQpy [10]. Based on the defined nominal values of the HR (see Tab. 1), the parameter range is defined by ±20 % deviation from these values. In addition to the ambient temperature, the lengths and diameters of the neck and cavity are also taken into account. Since the behaviour of the HR in the defined parameter range is to be investigated and not the influence of uncertain input parameters, e.g. through measurements, a uniform distribution $\mathcal{U}$ is assumed for all parameters.

**Table 1:** The range of variability of the Helmholtz resonator parameters (input values)

| Parameter | Unit | Nominal value | Bound |
|---|---|---|---|
| $t$ | °C | 20 | $\mathcal{U}(16, 24)$ |
| $l_{\mathrm{c}}$ | mm | 50 | $\mathcal{U}(40, 60)$ |
| $d_{\mathrm{c}}$ | mm | 26 | $\mathcal{U}(20.8, 31.2)$ |
| $l_{\mathrm{n}}$ | mm | 5 | $\mathcal{U}(4, 6)$ |
| $d_{\mathrm{n}}$ | mm | 3 | $\mathcal{U}(2.4, 3.6)$ |

The PCE surrogate models for both acoustic quantities are based on a total polynomial basis with a polynomial degree of 3 and a selected number of 112 training samples. This is based on a total Sobol index convergence study in a frequency range from 1 Hz to 1500 Hz with a resolution of 1 Hz. The accuracy of the surrogate model is also shown in Fig. 3, where the resonance frequency has a relative deviation of $\varepsilon_{f_{\mathrm{res}}} = 0.81$ % to the measurement. The relative deviation for the maximum absorption is $\varepsilon_{max(\alpha)} = 0.17$ %.

In Fig. 4 the Sobol indices of the total order $S_{\mathrm{T}_i}$ and the first order $S_i$ are shown for the resonance frequency $f_{\mathrm{res}}$ and the maximum of the absorption coefficient $\max(\alpha)$. The Sobol indices ($S_i$, $S_{\mathrm{T}_i}$) are approximately the same for both acoustic variables, which means that the parameters of the acoustic variables almost do not interact ($\sum S_i \approx 1$). It can also be seen for both acoustic quantities that the temperature $t$ has the least influence in relation to the other variables in the considered parameter range. The resonance frequency shows a sensitive behaviour due to the cavity diameter $d_{\mathrm{c}}$ and the neck diameter $d_{\mathrm{n}}$. In contrast, the lengths of the neck and the cavity have a much weaker influence. Of all the parameters, the neck diameter has the greatest influence on the maximum absorption behaviour.

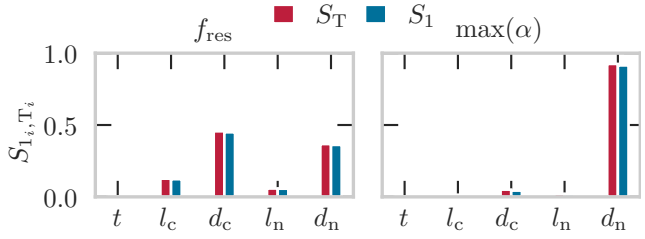


**Figure 4:** First and total order Sobol indices for **left**: resonance frequency and **right**: maximum absorption level

## Summary and outlook

This conference paper first presents the analytical description of a classical Helmholtz resonator. In order to validate the analytical model, a Helmholtz resonator made of aluminium was designed and the absorption behaviour was measured according to ISO 10534-2. In addition, a 2D simulation model was designed for validation, which is based on the same constitutive laws in the neck domain as the TMM model. The semi-analytical model (TMM) shows a high degree of accuracy compared to the measured and numerically calculated absorption behaviour. To determine the parameters that have a sensitive influence on the resonance frequency and the maximum absorption behaviour, an efficient global sensitivity approach is chosen. Instead of calculating the variance-based Sobol indices via sampling based methods, a surrogate model based on polynomial chaos expansion is used. For both acoustic variables, the model shows almost additive behaviour. While the resonance frequency depends mainly on the diameter of the neck and the cavity, the absorption depends almost exclusively on the neck diameter. The temperature has a negligible influence on both acoustic quantities in the defined parameter range.

An extension of the model to multi-neck HR can contribute to the robust development of acoustic metamaterials. In this context, additive manufacturing processes could also play an important role due to their great design flexibility. Consequently, the model would need to be extended and thoroughly analysed to evaluate the effects of the process parameters on the acoustic properties.

## Acknowledgements

The authors would like to thank our colleagues S. Hoffmann for preparing the samples and J. Schultz for the discussions on the sensitivity methods.

## Funding Acknowledgements

Funded by the Deutsche Forschungsgemeinschaft (DFG, German Research Foundation) – project number: 508318707

## References

[1] J. M. Sinapius: Adaptronik: Prinzipe - Funktionswerkstoffe - Funktionselemente - Zielfelder mit Forschungsbeispielen. Springer Berlin Heidelberg, 2018, pp. 375-450.

[2] J.-F. Allard: Propagation of Sound in Porous Media: Modelling Sound Absorbing Materials. Springer Netherlands, Dordrecht, 1993, pp. 48-78.

[3] ISO 10534-2:2023: Acoustics - Determination of acoustic properties in impedance tubes - Part 2: Two-microphone technique for normal sound absorption coefficient and normal surface impedance.

[4] P. R. White, M. H. Tan and J. K. Hammond: Analysis of the maximum likelihood, total least squares and principal component approaches for frequency response function estimation. In: Journal of Sound and Vibration, Vol. 290, Issues 3-5, 2006, pp. 676–689.

[5] M. Dietz: Aerodynamik des Fliegens: Von den Grundlagen bis zur Flugzeugauslegung. Springer Berlin Heidelberg, Berlin, Heidelberg, 2024, pp. 3–8.

[6] H. D. Baehr and K. Stephan: Einführung. Technische Anwendungen. In: Wärme- und Stoffübertragung. Springer Berlin Heidelberg, Berlin, Heidelberg, 2016, pp. 1–119

[7] L. Jaouen and F. Chevillotte: Length correction of 2D discontinuities or perforations at large wavelengths and for linear acoustics. In: Acta Acustica United With Acustica, Bd. 104, 2018, pp. 243–250

[8] K. U. Ingard: Noise Reduction Analysis, 2009

[9] B. Sudret: Polynomial chaos expansions and stochastic finite element methods. In: Risk and Reliability in Geotechnical Engineering,(Chap. 6), K.-K. Phoon & J. Ching (Eds.), pp. 265-300, CRC Press.

[10] A. Olivier, D. G. Giovanis, B. S. Aakash, M. Chauhan, L. Vandanapu and M. D. Shields: UQpy: A general purpose Python package and development environment for uncertainty quantification. In: Journal of Computational Science, 2020.

[11] D.-Y. Maa: Potential of microperforated panel absorber. Journal of the Acoustical Society of America, 1998, 104 (5), pp. 2861-2866.

[12] T. Okuzono, T. Nitta and K. Sakagami: Note on microperforated panel model using equivalent-fluid-based absorption elements, AST, 2019.

[13] I. B. Crandall, Theory of Vibrating Systems and Sound, D. Van Nostrand Company, New York, 1926.

[14] Y. Guo, S. Allam and M. Abom: Micro-perforated plates for vehicle applications, Proc. Internoise 2008, 2008